Supplementary Figure. 1

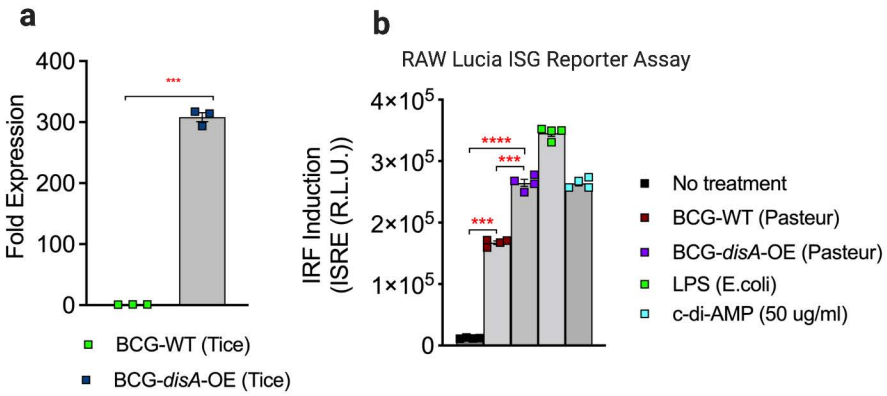

Supplementary Figure 1. Confirmation of *M.tb-disA* overexpression BCG-*disA*-OE and induction of IRF signaling. a. mRNA level of *disA* in log-phase BCG cultures relative to *M. tuberculosis sigA* (Rv2703) (n= 3 independent biological replicates). **b.** IRF3 induction measured in RAW-Lucia ISG reporter macrophages. IRF quantification was carried out in culture supernatant of macrophages infected at a MOI of 20:1 for 24 hr (n= 4 independent biological replicates). Data are presented as mean values ± S.E.M. Statistical analyses done using 2-tailed Student's t-test (*** P < 0.001, **** P < 0.0001).

Supplementary Figure. 2

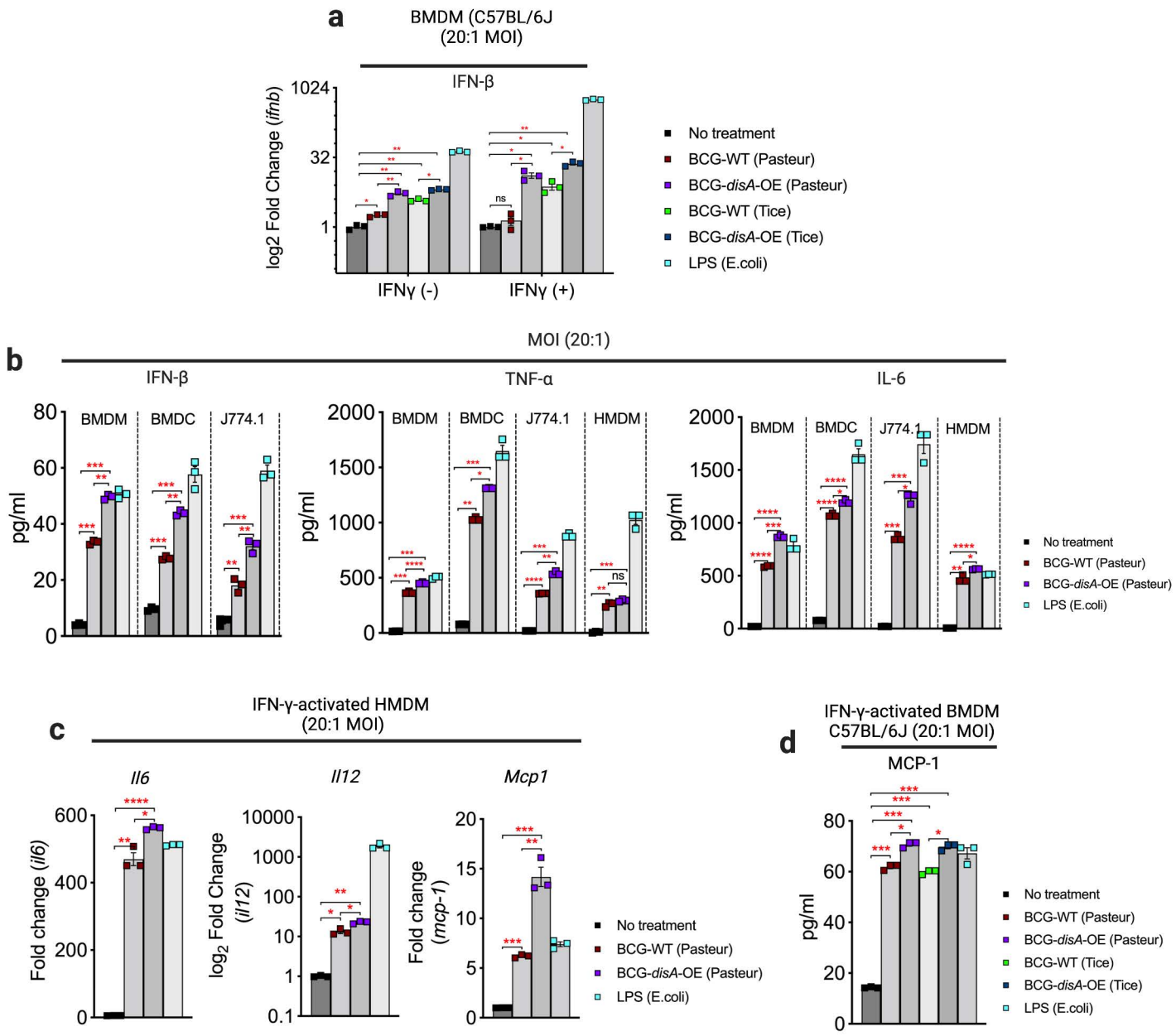

Supplementary Figure 2. BCG-*disA*-OE elicits stronger IFN-β, pro-inflammatory cytokines and chemokines than BCG-WT in primary human and murine macrophages and dendritic cells. a. IFN-β levels in resting and IFN-γ primed BMDMs. **b.** IFN-β, TNF-α, and IL-6 levels in human and murine primary macrophages, murine primary dendritic cells and J774.1 murine macrophage cell line . **c.** mRNA levels of *Il6*, *Il12* and *Mcp1* in IFN-γ primary human macrophages relative to β-actin. **d.** MCP-1 levels in IFN-γ primed murine primary macrophages. Cytokines and chemokine levels were measured by ELISA after 24 hr exposures at a MOI of 20:1. Data are presented as mean values ± S.E.M (n= 3 independent biological replicate experiments). Gene expression analyses of cytokines and chemokines was done after 6 hr exposure. Statistical analyses done using 2-tailed Student's t-test; (* P < 0.05, ** P < 0.01, *** P < 0.001, **** P < 0.0001).

Supplementary Figure.3

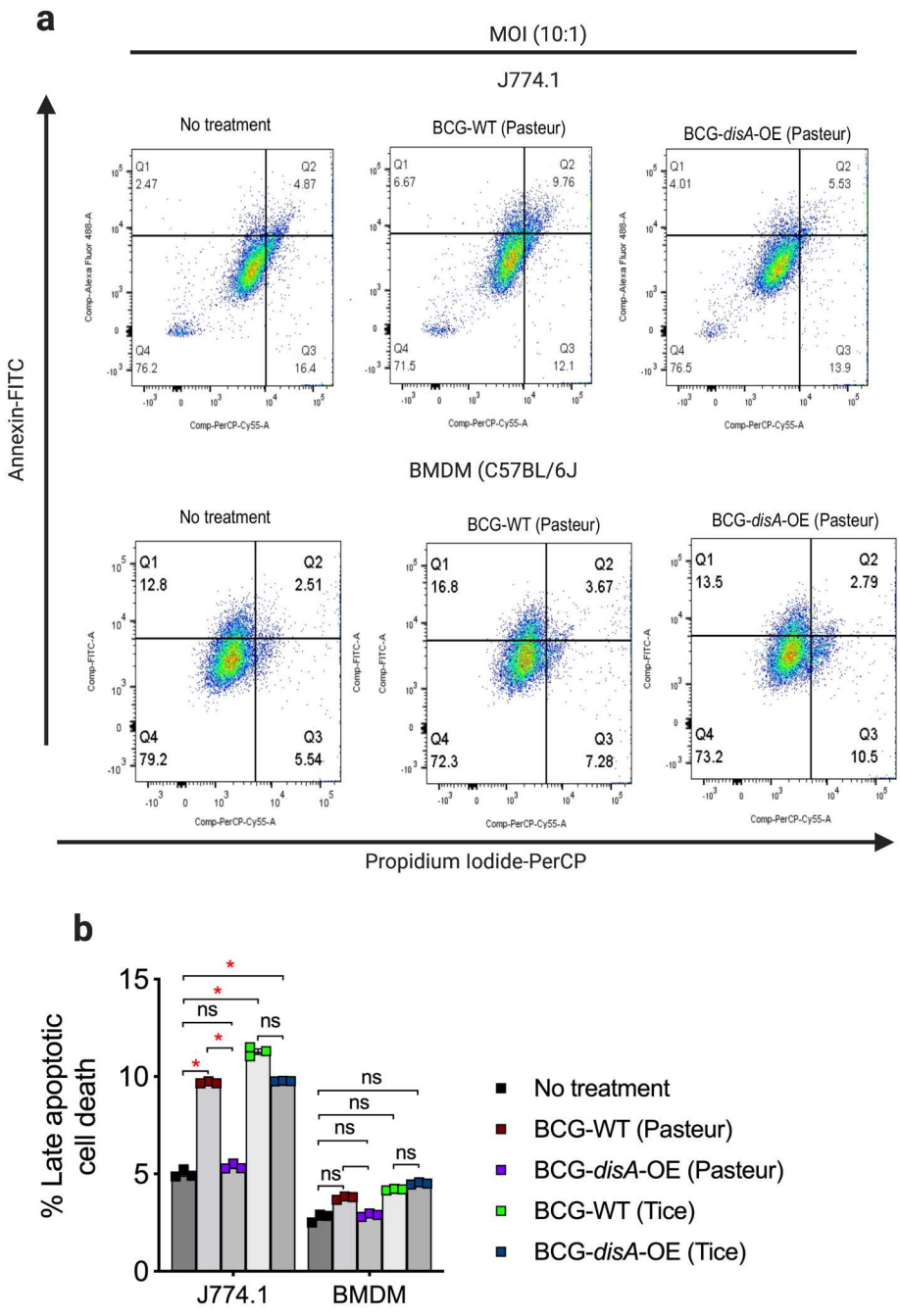

Supplementary Figure 3. BCG-*disA*-OE is less toxic to macrophages than that of WT-BCG. a-b. Percentage late apoptotic murine primary macrophages and J774.1 macrophage cell line. Data was collected after 24 hr exposure at a MOI of 20:1 as determined by flow cytometry. Data are presetned as mean values ± S.E.M. (n = 3 independent biological replicate experiments). Statistical analysis done using 2-tailed Student's t-test (* P < 0.05).

Supplementary Figure. 4

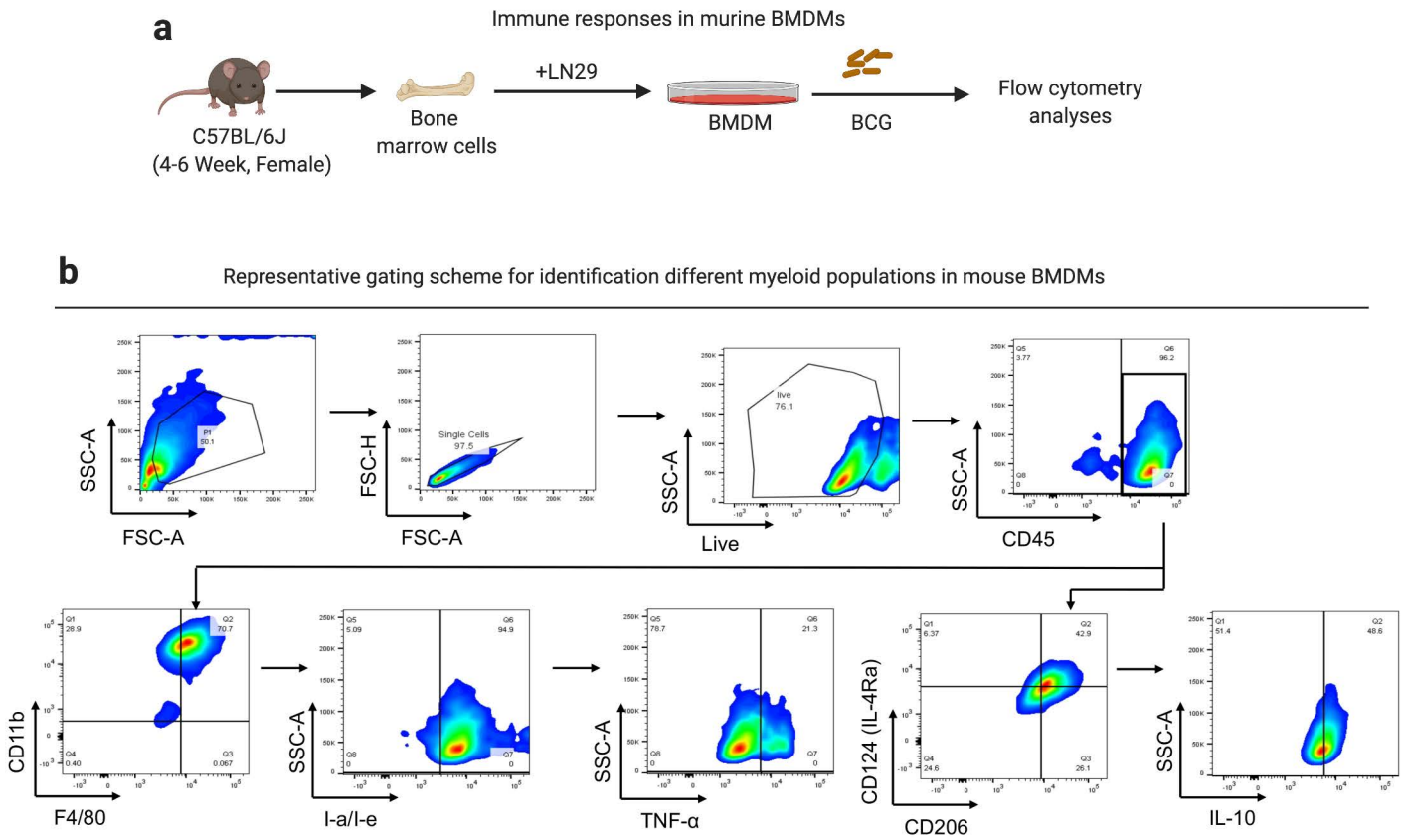

Supplementary Figure 4. Representative gating scheme for identification of different myeloid populations in mouse BMDMs. a. Schematic of generation of BMDMs. **b.** Representative gating scheme for identification of different myeloid cells. Briefly, leukocyte lineage was selected by gating SSC-A against $CD45^+$ populations on live cells. $CD11b^+F4/80^+$ macrophages were identified out of $CD45^+$ population. $CD11b^+F4/80^+$ macrophages were divided into MHC class II (I-a/I-e) and $CD124^+CD206^+$ populations. Expression of TNF-α (M1-like macrophages) and IL-10 (M2-like macrophages) were determined on MHC class II subsets and $CD124^+CD206^+$ subsets respectively (**Related to Fig. 2a**).

Supplementary Figure. 5

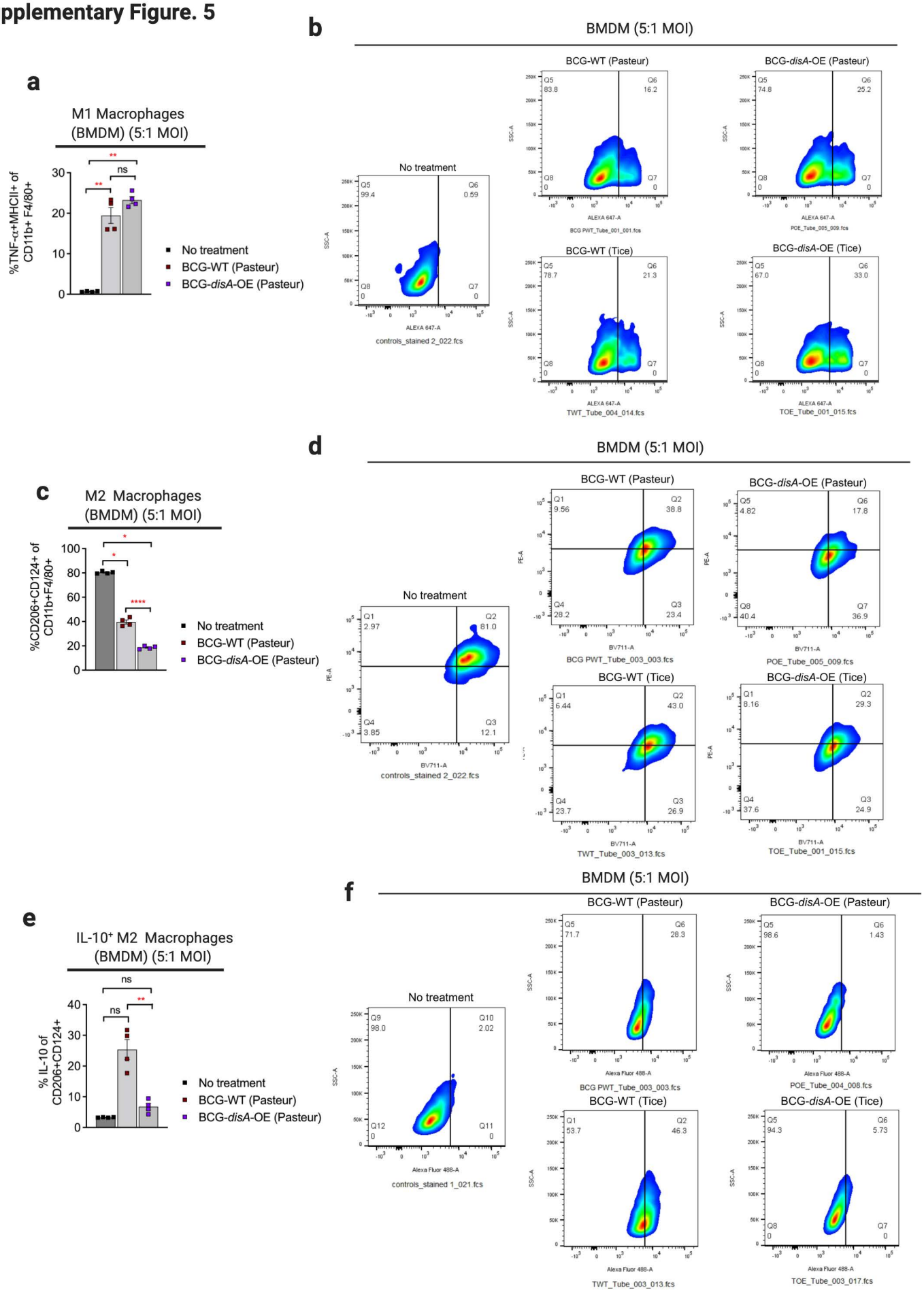

Supplementary Figure 5. BCG-*disA*-OE induces macrophage reprogramming and favors stronger inflammatory macrophage shift in murine BMDMs. a-b. Percentage TNF-α⁺ M1-like macrophages (MHC Class II⁺CD11b⁺F4/80⁺) and corresponding representative FACS plots. **c-d.** Percentage M2-like macrophages (CD206⁺CD124⁺) and corresponding representative FACS plots. **e-f.** Percentage IL-10⁺ M2-like macrophages (CD206⁺CD124⁺) and corresponding representative FACS plots. Data are presented as mean values ± S.E.M. (n= 4 independent biological replicate experiments). Statistical analyses done using 2-tailed Student's t-test (* P < 0.05, ** P < 0.01, *** P < 0.001, **** P < 0.0001). **(Related to Fig. 2a)**.

Supplementary Figure 6

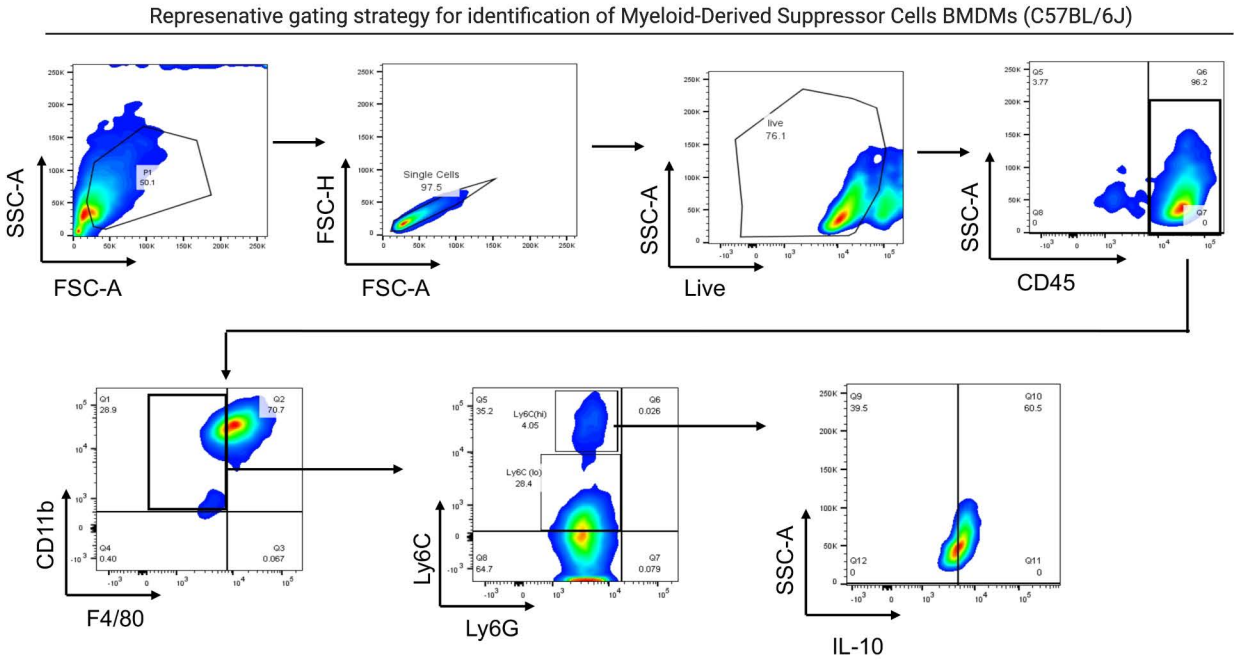

Supplementary Figure 6. Gating scheme showing identification of myeloid-derived suppressor cell (MDSC) populations in primary mouse macrophages after BCG exposure. Leukocyte lineage was determined on live cells by gating SSC-A against CD45^{+} myeloid cells. Myeloid cells were differentiated into CD11b^{+}F4/80^{+} macrophages out of which CD11b^{+}F4/80^{-} myeloid population was divided into Ly6C and Ly6G. Next, the Ly6C$^{(hi)}$Ly6G^{-} immunosuppressive myeloid-derived suppressor cell populations were looked for IL-10 positivity (**Related to Fig. 2a**).

Supplementary Figure. 7

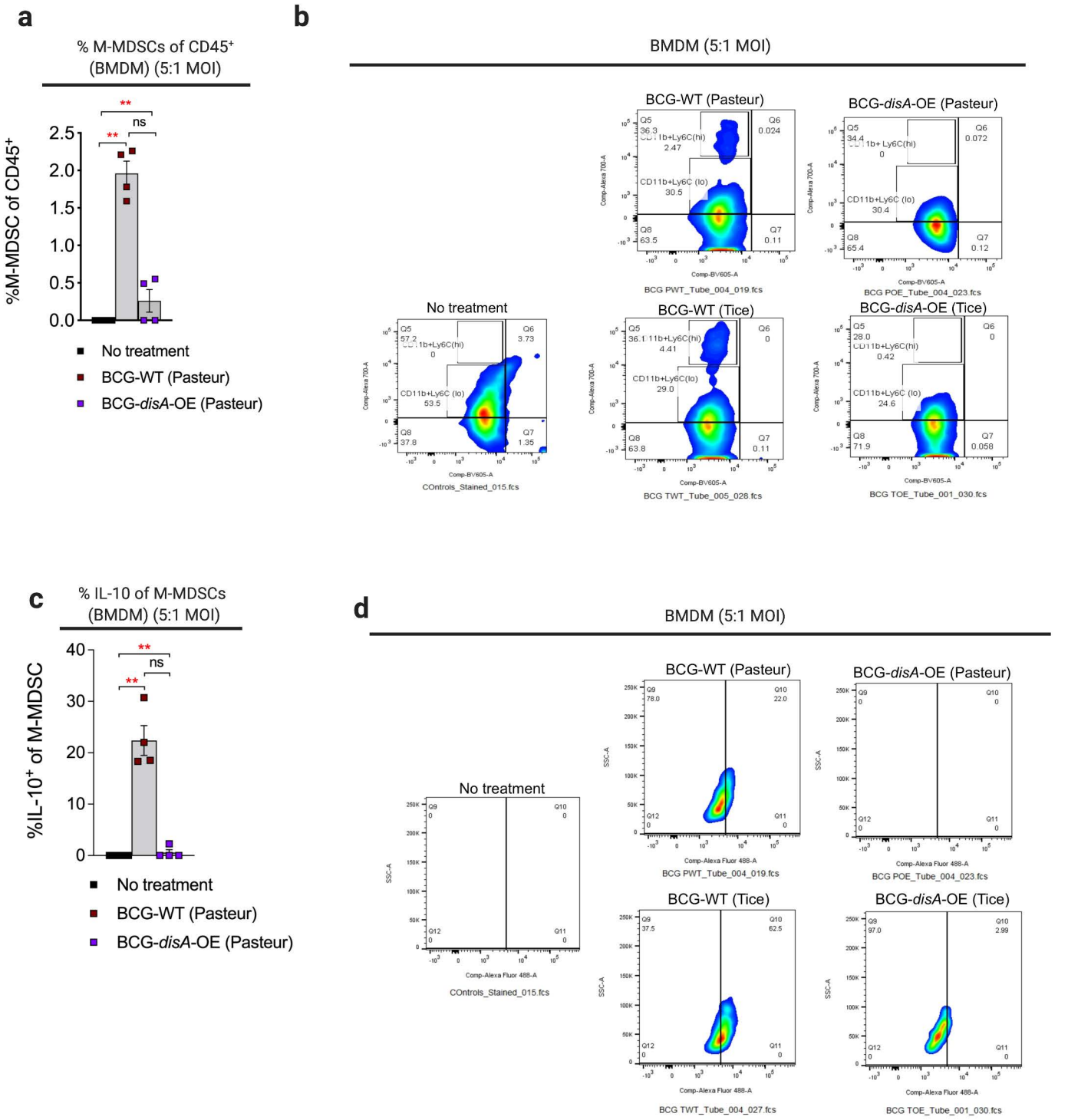

Supplementary Figure 7. Immunosuppressive monocytic-MDSC (M-MDSC) populations in murine primary macrophages after BCG exposure. a-b. Percentage of M-MDSCs and corresponding representative FACS plot. **c-d.** Percentage of IL-10^{+} immunosuppressive M-MDSCs and corresponding representative FACS plots. Data are presented as mean values ± S.E.M. (n = 4 independent biological replicate experiments). Statistical analyses done using 2-tailed Student's t-test (* P < 0.05, ** P < 0.01, *** P < 0.001, **** P < 0.0001). (**Related to Fig. 2a**).

Supplementary Figure. 8

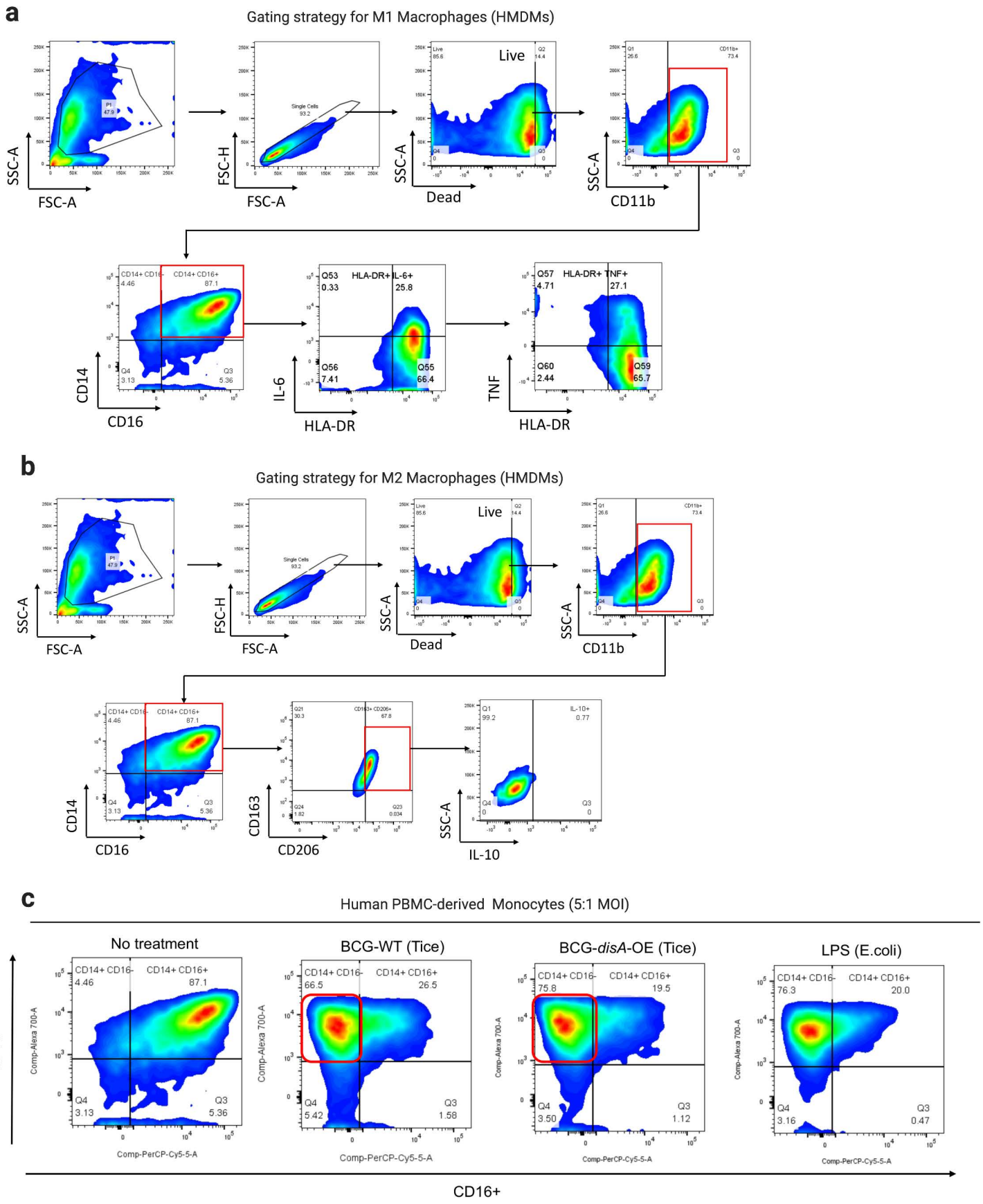

Supplementary Figure 8. BCG-*disA*-OE strongly induces inflammatory human macrophages. a. Gating strategy for M1-like macrophages **b.** Gating strategy for M2-like macrophages. **c.** Representative FACS plot showing percentage of classically activated ($CD14^+CD16^-$) macrophages after BCG exposure. **(Related to Figure 2b).**

Supplementary Figure. 9

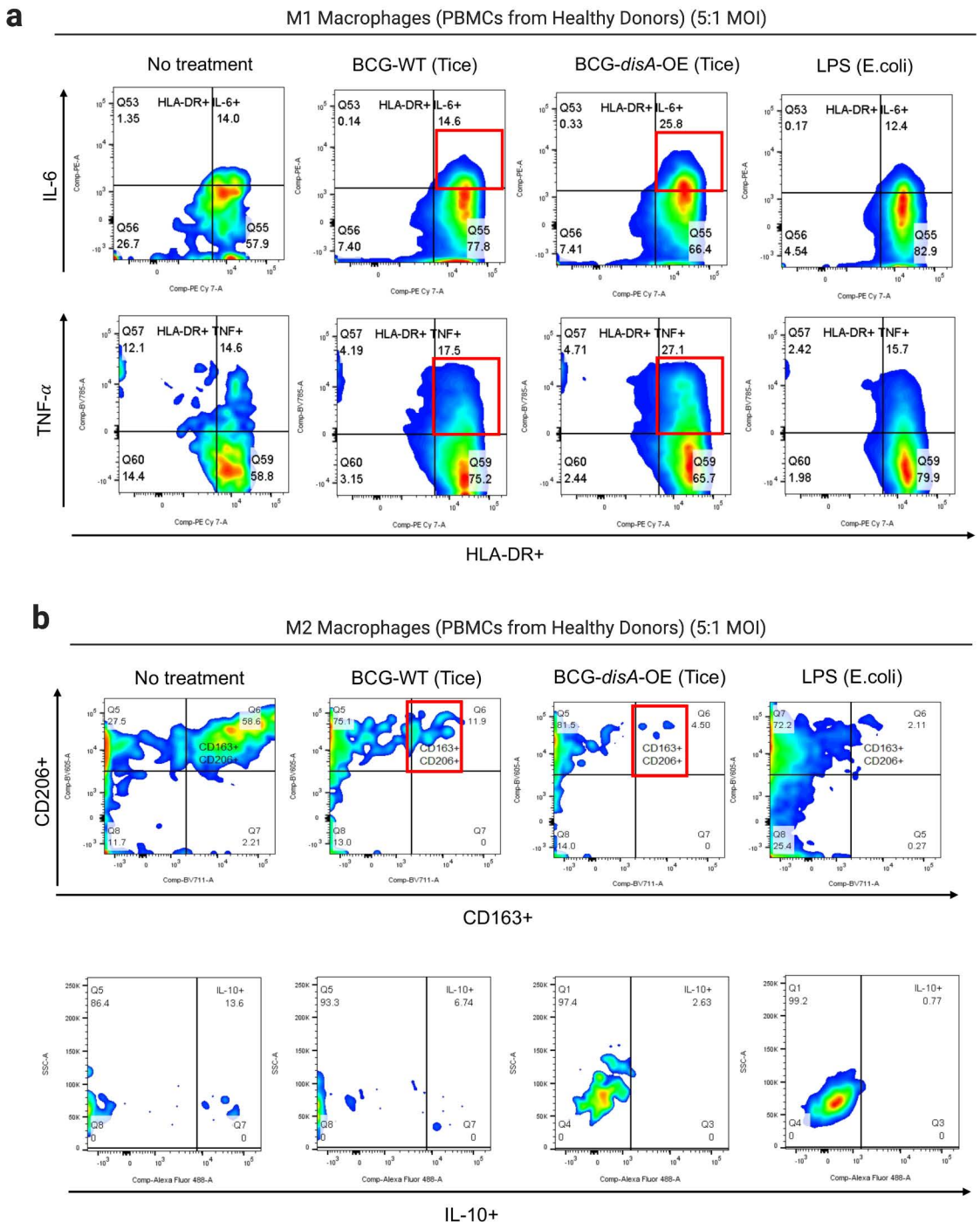

Supplementary Figure 9. BCG-*disA*-OE causes strong inflammatory macrophage shift in human primary macrophages. a. FACS plot showing inflammatory M1-like macrophages ($CD14^{+}CD16^{-}$). **b.** FACS plots showing immunosuppressive M2-like macrophages ($CD206^{+}CD163^{+}$ of $CD14^{+}CD16^{+}$) after BCG exposure. (**Related to Figure 2b**).

Supplementary Figure. 10

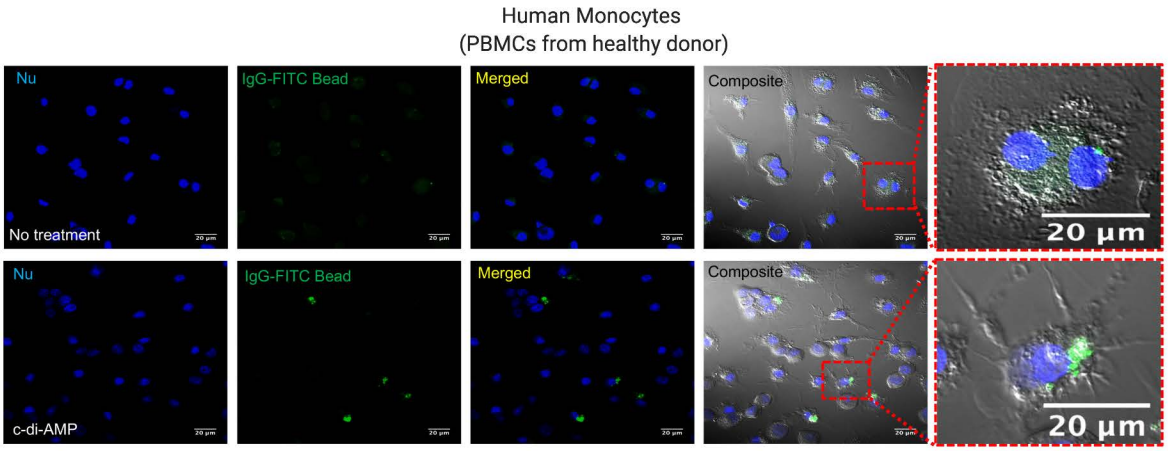

Supplementary Figure 10. STING agonist c-di-AMP causes induction of macrophage activation. Human macrophages were transfected with c-di-AMP for 24 h and phagocytosis of FITC-labeled IgG opsonized latex beads (green) was visualized using confocal microscopy on live cells. Hoechst was used for nuclear staining (blue). Images were acquired using LSM700 confocal microscope at 63X magnification. Images were process using Fiji software. Similar results were observed across two (n= 2) independent biological replicate experiments.

Supplementary Figure 11

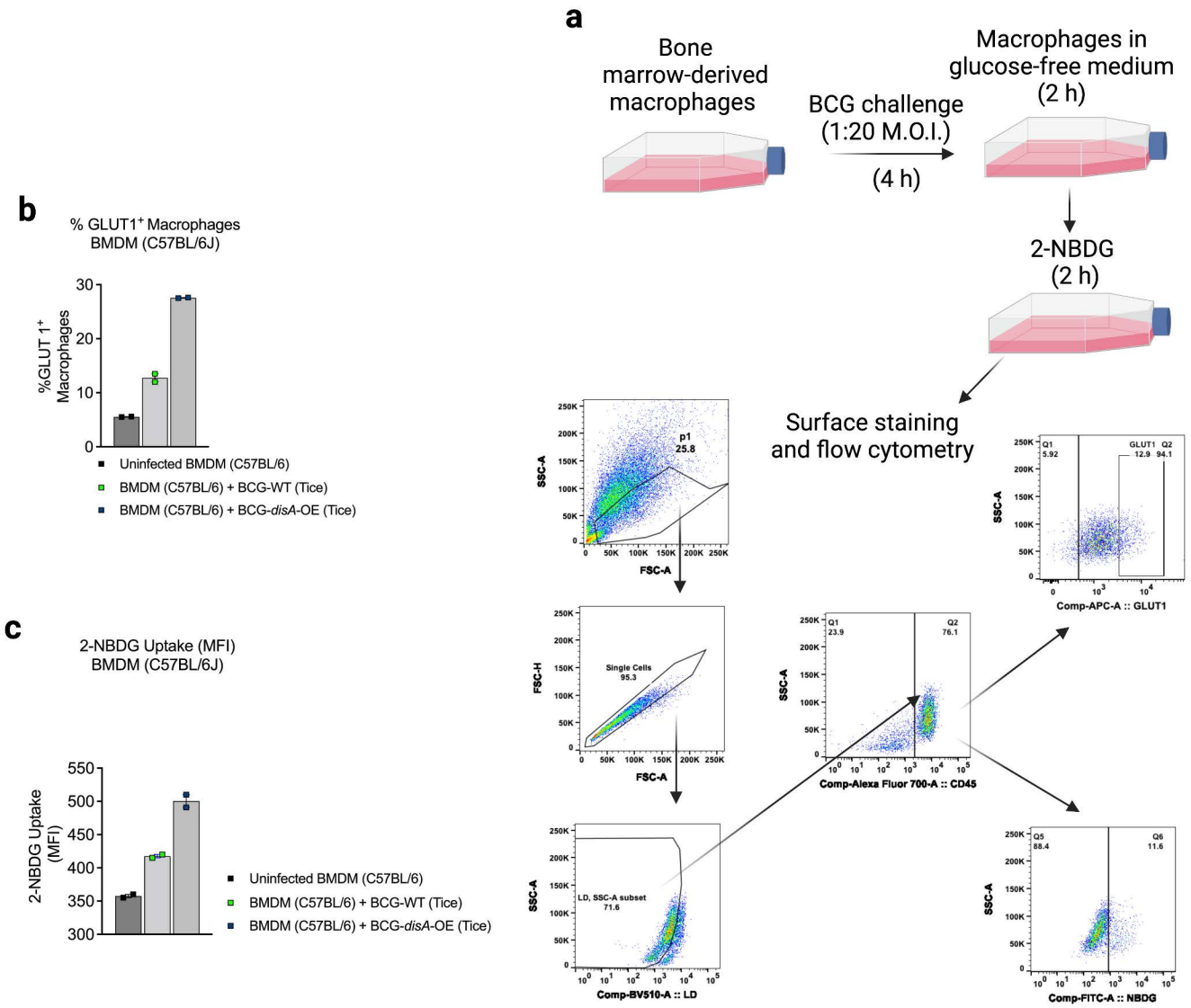

Supplementary Figure 11. BCG induced differential glucose uptake in bone-marrow-derived macrophages (BMDMs). a. Experimental layout showing the strategy employed to determine intracellular uptake of fluorescent glucose. Briefly macrophages were infected at a ratio of 1:20 (macrophaghe vs BCG ratio) in the presence of glucose-free medium followed by addition of exogenous 2-NBDG. Macrophages were subseqently stained for GLUT1 and were investigated using flow cytometry. **b-c.** Bar diagram showing induced expression of GLUT1 and intracellular fluorescent 2-NBDG in BMDMs following infection by BCG strains. Data are represented as mean values ± S.E.M. (n= 2 independent biological replicate experiments). Data analyses were carried out using FACSDiva (v 9.0), Flowjo (v10) and Graphpad Prism software (v 9.0).

Supplementary Figure. 12

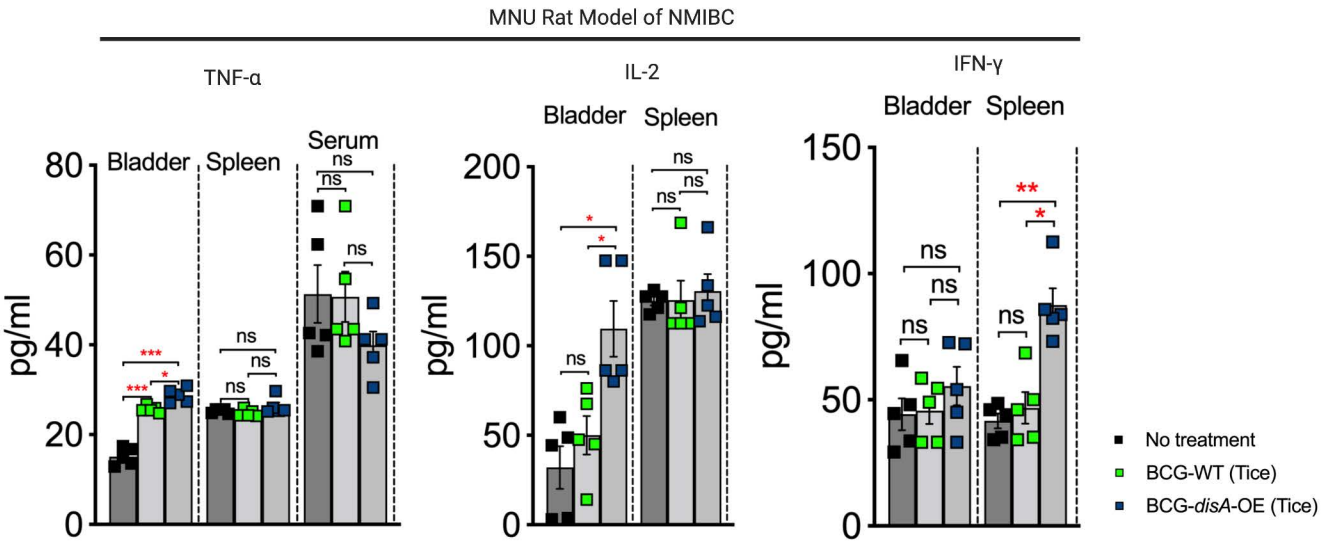

Supplementary Figure 12. Cytokine changes elicted by BCG-WT and BCG-*disA*-OE in the orthotopic, carcinogen-induced rat model of NMIBC. M1-like macrophage cytokines in MNU rat bladder, spleen and blood serum at necropsy at week 24 (n=5 animals / group). Data are presented as mean values ± S.E.M. Statistical analyses done using 2-tailed Student's t-test (* P < 0.05, ** P < 0.01, *** P < 0.001). (**Related to Figure 5**).

Supplementary Figure. 13

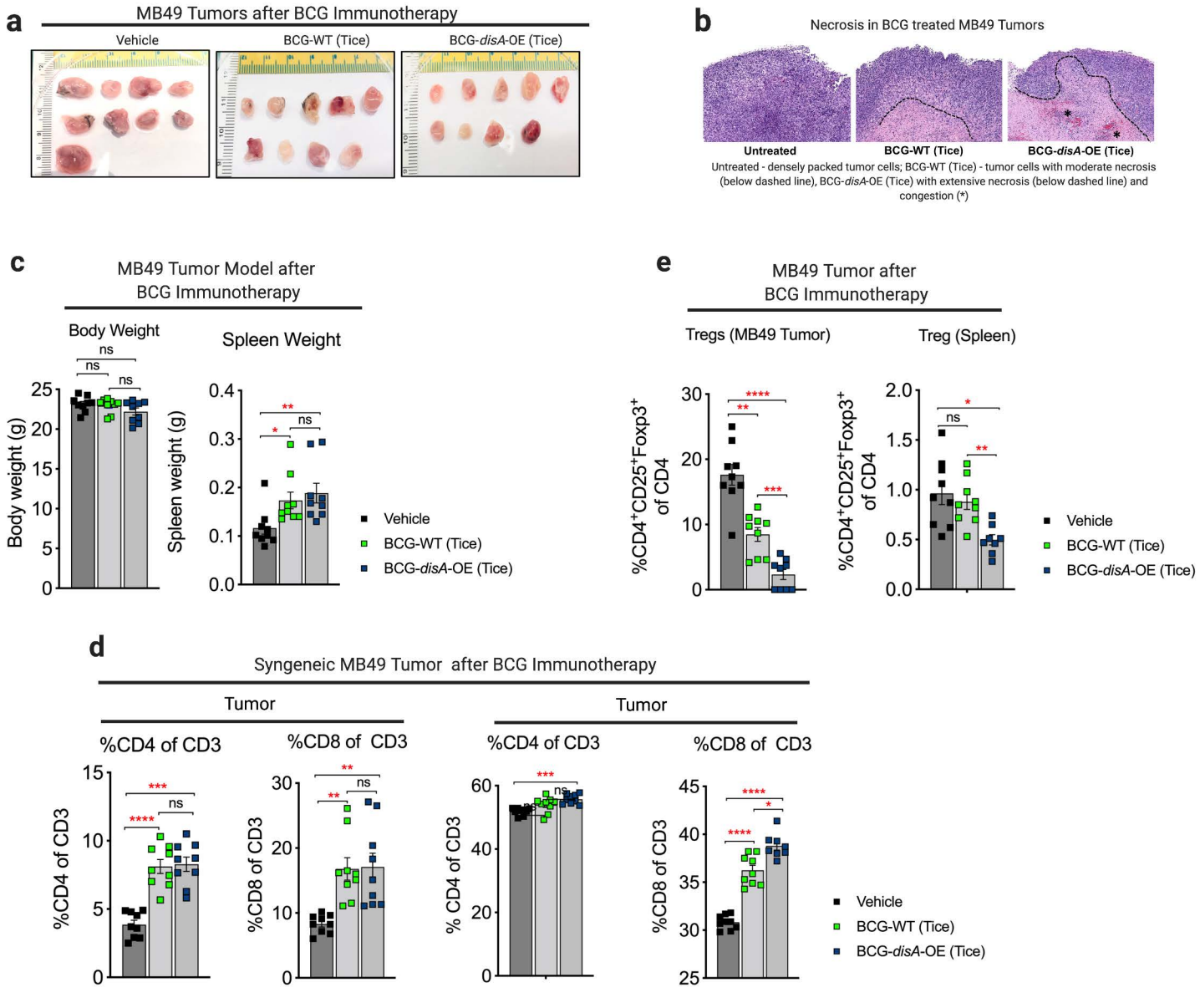

Supplementary Figure 13. BCG-*disA*-OE causes reduced tumor outgrowth, greater Teffector recruitment, and reduced Tregs in heterotopic syngeneic MB49 mouse model of urothelial cancer. a. Tumors at necropsy on day 21(n= 9 animals / group). **b.** Representative H & E staining showing necrotic areas and congestion in MB49 tumors. Similar obeservations were made in randomly selected 3 (n=3) tumor tissue slides per group. **c.** Body and spleen weight after necropsy (n=9 animals/group). **d.** Increased percentage of tumor infiltrating $CD4^+$ and $CD8^+$ T cells in MB49 tumors and mouse spleens (n=9 animals / group). **e.** Decreased percentage of $CD4^+$ Treg in tumor and spleen of MB49 tumor bearing animals (n=9 animals/group). Data are represented as mean values ± S.E.M. Statistical analyses done using 2-tailed Student's t-test (* P < 0.05, ** P < 0.01, **** P < 0.0001). (**Related to Fig 6**).

Supplementary Figure.14

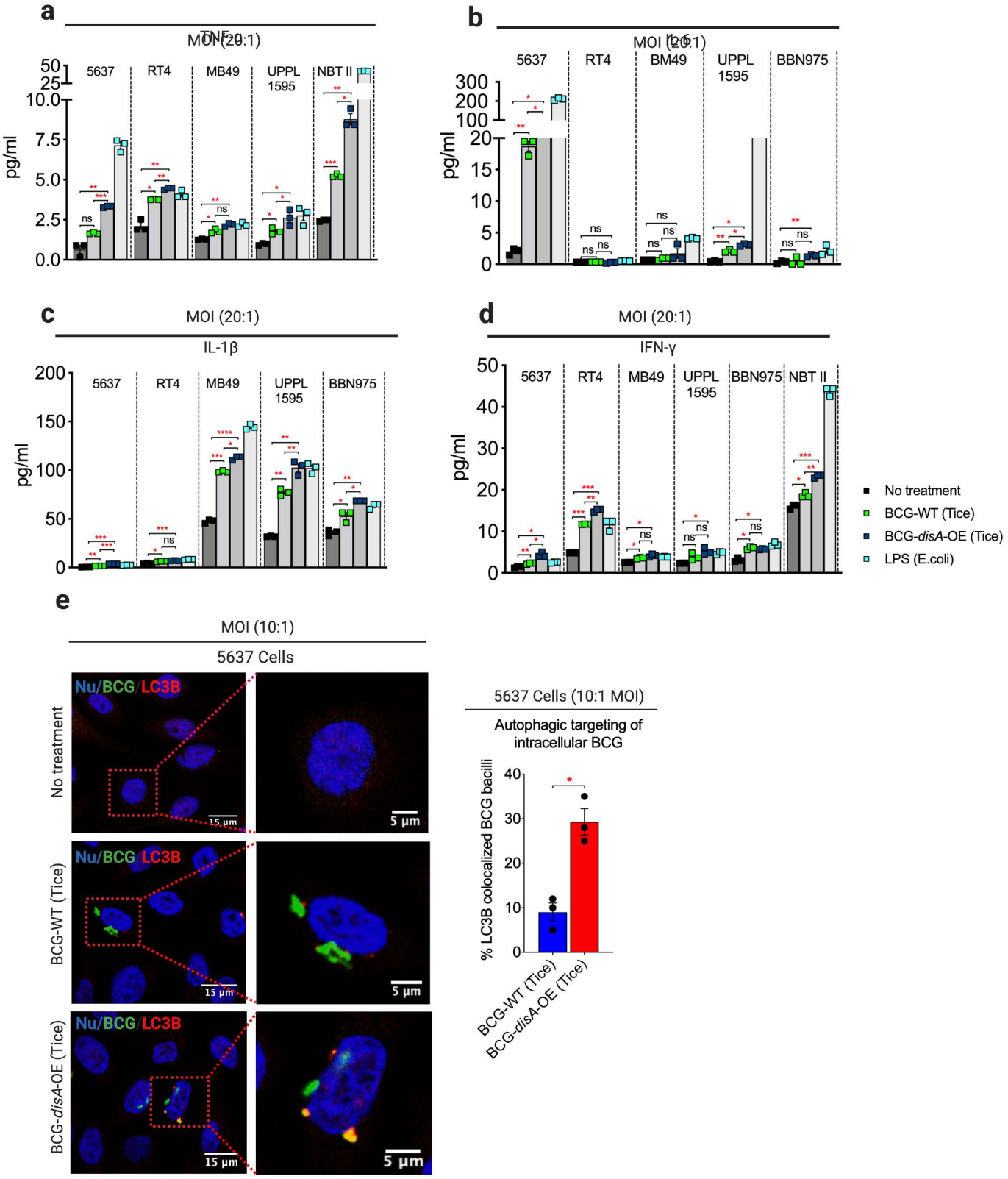

Supplementary Figure 14. BCG-*disA*-OE elicits greater pro-inflammatory cytokine responses and autophagy than BCG-WT in human and murine urothelial carcinoma cells. a-d. TNF-α, IL-6, IL-1β and IFN-γ levels in urothelial carcinoma cell lines: 5637 (human epithelial high grade carcinoma), RT4 (human transitional low grade carcinoam cells), NBT II (carcinogen-induced rat tumor), MB49, UPPL1595, and BBN975 (all carcinogen-induced mouse tumors). Cytokine levels were measured by ELISA after 24 hr exposures at MOI of 20:1. Data are presented as mean values ± SEM (n = 3 independent biological replicate experiments). **e.** Autophagy induction in the 5637 human urothelial carcinoma cells in representative confocal photomicrographs (n=3 independent biological replicate experiments). Colocalization of FITC-labeled BCG strains (green), LC3B autophagic puncta (red) appears in yellow; nuclei are blue. Cells were fixed using 4% paraformaldehyde 3h after infection (MOI 10:1), and images obtained with an LSM700 confocal microscope and Fiji software processing. Satistical analyses done using 2-tailed Student's-test (* $P < 0.05$, ** $P < 0.01$, *** $P < 0.001$, **** $P < 0.0001$). Data shown are for BCG-Tice; similar findings were observed for BCG-Pasteur.

Supplementary Figure. 15

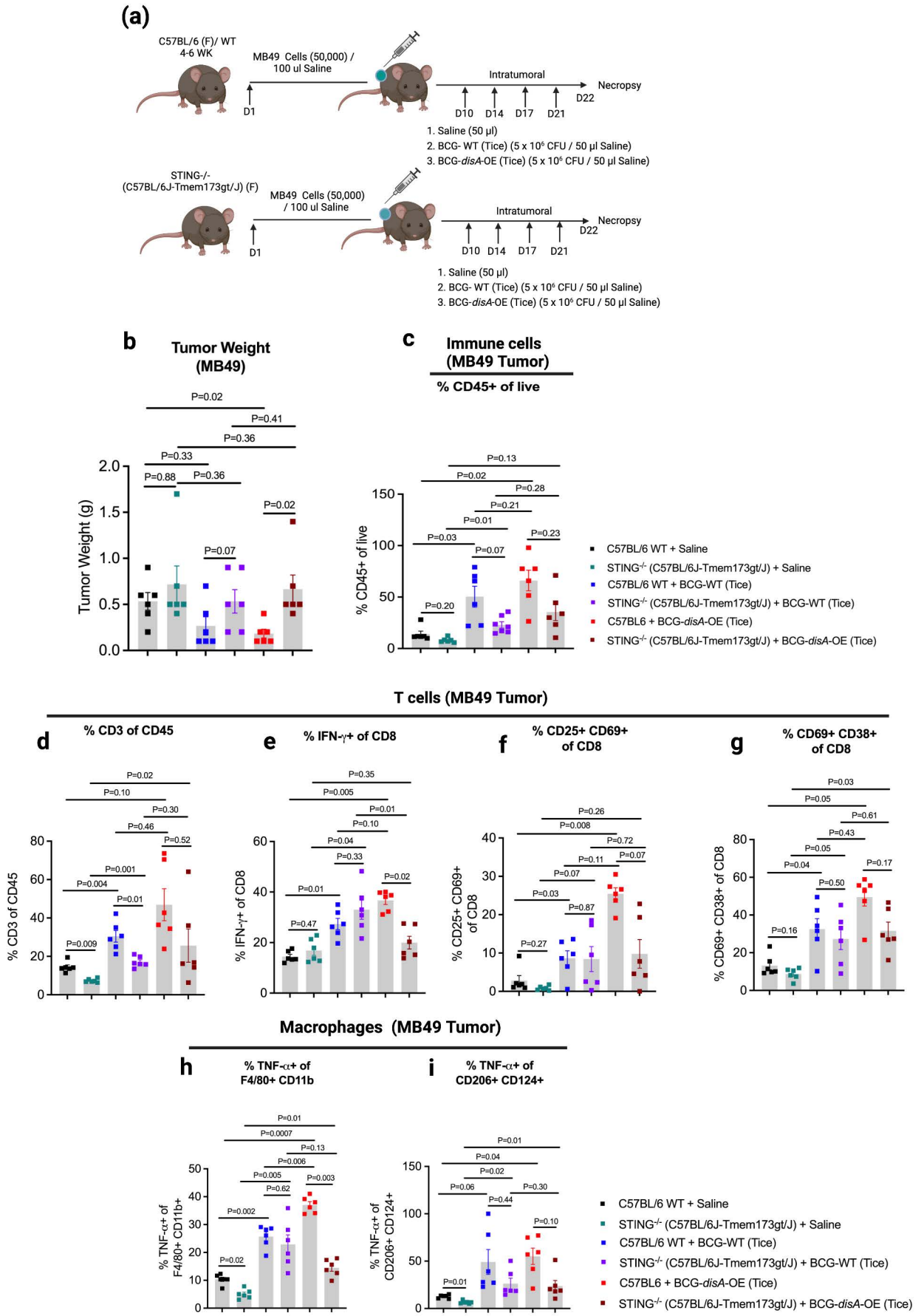

Supplementary Figure 15. Improved antitumor efficacy of BCG-*disA*-OE is STING-dependent. a. Schematic diagram of MB49 syngeneic mouse model of urothelial tumor. **b.** tumor weight at the time of necropsy. **c.** total CD45$^+$ immune cells in tumors. **d.** total tumor infiltrating CD3$^+$ lymphocytes. **e.** IFN-γ$^+$ tumor infiltrating CD8$^+$ T cells. **f-g.** activated CD8$^+$ T cells. **h.** tumor infiltrating inflammatory macrophages, and **i.** differential abundance of TNF$^+$ immunosuppressive macrophages in MB49 tumors after necropsy. Data are presented as mean values ± S.E.M. (n= 6 animals / group). Statistical analyses done using 2-tailed Student's t-test (* P < 0.05, ** P < 0.01, *** P < 0.001, **** P < 0.0001).

Supplementary Figure. 16

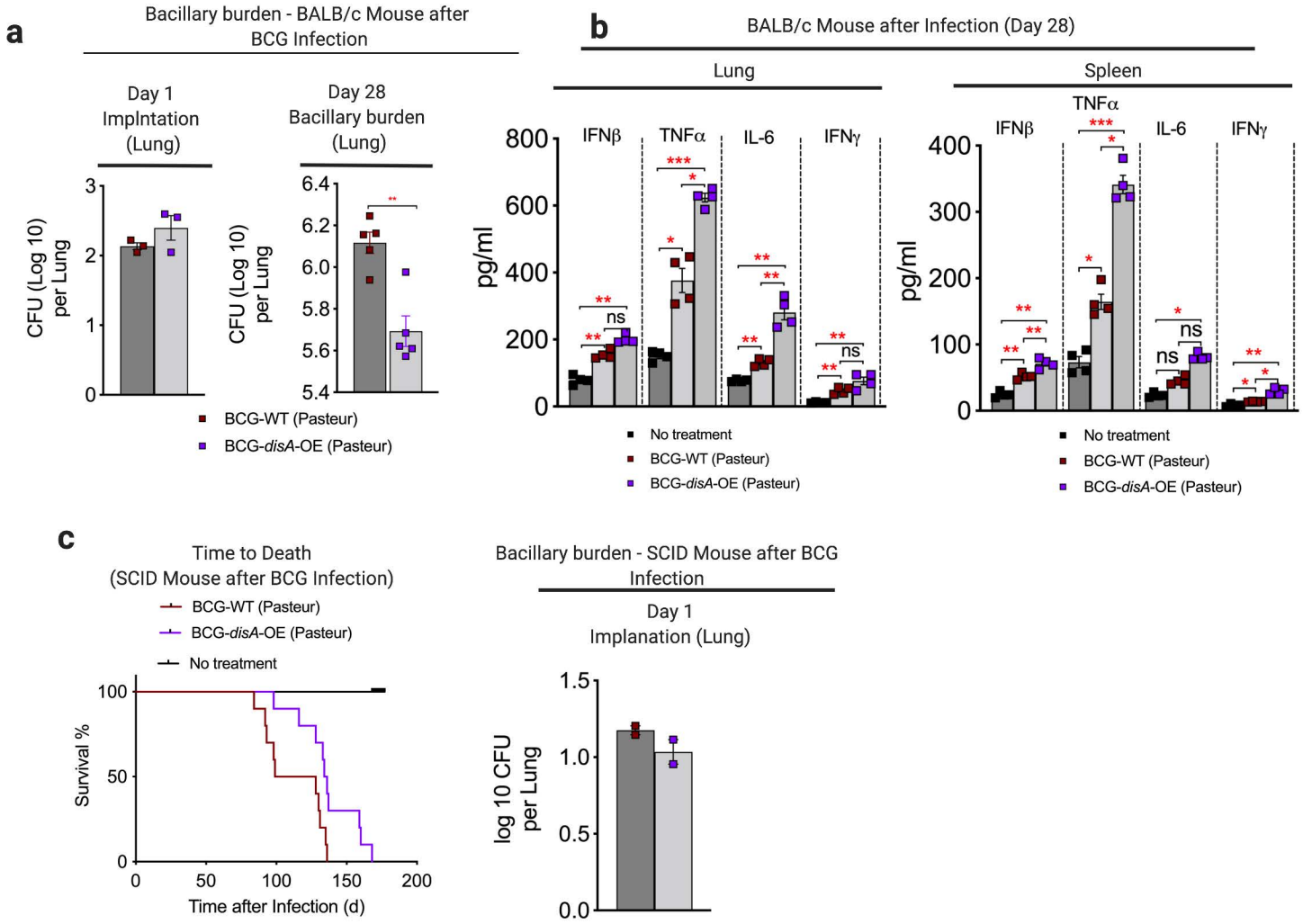

Supplementary Figure 16. BCG-*disA*-OE (Pasteur) is less pathogenic that BCG-WT in mouse models and elicits stronger proinflammatory cytokines in vivo. a. Lung colony forming unit (CFU) counts at day 1 (N= 3 animals / group) and day 28 (n= 5 animals / group). Data are presented as mean values ± S.E.M. **b.** Levels of the pro-inflammatory cytokines IFN-β, TNF-α, IL-6, and IFN-γ in mouse lungs and spleens determined by ELISA at day 28 (n= 4 animals / group). Data are preesented as mean values ± S.E.M. **c.** Percent survival of SCID mice following low dose challenge (n= 10 animals / group). The day 1 lung CFU counts (n= 2 animals / group) are shown at right. Statistical analyses done using 2-tailed Student's t-test (* P < 0.05, ** P < 0.01, *** P < 0.001, **** P < 0.0001). (**Related to Fig. 7**)

Supplementary Table. 1: List of bacterial strains, cell lines, plasmids and antibodies used in the study

Name	Description/Source
Bacterial strains	
***M. tuberculosis* strain**	
Mtb-CDC1551	Wild-type *M. tuberculosis*
***M. bovis* BCG strains**	
BCG Pasteur	*M. bovis* BCG Pasteur
BCG-*disA*-OE (Pasteur)	BCG Pasteur strain overexpressing *disA* (MT3692) of *M.tb*
BCG Tice	*M. bovis* BCG Tice
BCG-*disA*-OE (Tice)	BCG Tice strain overexpressing *disA* (MT3692) of *M.tb*
***E. coli* strain**	
DH5-α	Competent *E. coli* (High Efficiency)
Cell lines	
Urinary bladder carcinoma cells	
RT4 (ATCC ® HTB-2™)	Human low grade urothelial cancer
5637 (ATCC® HTB-9™)	Human high-grade urothelial cancer
NBT-II (ATCC® CRL-1655™)	N-butyl-N-(4-hydroxybutyl) nitrosamine induced tumor cell line in Rattus norvegicus Nara Bladder Tumor No. 2
MB49 (Cat. SSC148, EMD Millipore)	DMBA [7,12-dimethylbenz[a]anthracene] induced murine urothelial carcinoma cells,
UPPL-1595	Luminal cell line established from a spontaneous primary bladder tumor in an Uroplakin-Cre driven PTEN/P53 knockout genetically engineered mouse model
BBN 975	Basal- cell line established from 0.05% N-Butyl-N-(4-hydroxybutyl) nitrosamine (BBN) induced murine urothelial cancer model
J28 (ATCC® HTB-1™)	high grade urothelial cancer
Reporter cells	

RAW-Lucia ISG (InvivoGen)	IFN Reporter Raw 264.7 murine macrophages		
Macrophage cell lines			
J774A.1 (ATCC® TIB67™)	Murine macrophage cell line		
Plasmids			
pSD5.hsp60	Mycobacterial expression plasmid with hsp60 promoter		
pSD5hsp60.MT3692	*disA* over-expression plasmid		
Confocal Microscopy Reagents			
Primary Antibodies			
Name	**Source**	**#Cat.**	**Dilution**
LC3B	Novus Biologicals	NB100-2220	1:200
P62/SQSTM1	Sigma-Aldrich	P0067	1:100
Secondary Antibodies			
Goat anti-Rabbit IgG Alexa Fluor Plus 647	Thermo Fisher Scientific	A32733	1:1000
Chemicals/Probes			
Fluorescein 5(6)-isothiocyanate (FITC)	Sigma-Aldrich	46950	
Hoechst 33342	Thermo Fisher Scientific	62249	
Flow Cytometry Reagents			
Antibodies (mouse BMDM study)			
anti-CD45 (clone 30-F11)	Biolegend	103128	1:200
anti-CD124 (I clone 015F8)	Biolegend	144804	1:50
anti-I-A/I-E (clone M5/114.15.2)	Biolegend	107645	1:200
anti-Ly6C (clone HK1.4)	Biolegend	128046	1:50
anti-CD11b (clone M1/70)	Biolegend	101206	1:200
anti-F4/80 (clone BM8)	Biolegend	123147	1:50
anti-Ly6G (clone 1A8)	Biolegend	127641	1:100
anti CD206 (clone C068C2)	Biolegend	141721	1:200
anti-TNF (clone MP6-XT22)	Biolegend	506341	1:100

anti- IL-10 (clone JES5-16E3)	eBioscience	505021	1:50
Anti-Glut1 (clone EPR3915)	Abcam	ab195020	1:50
Antibodies (HMDM study)			
anti-CD16 (clone 3G8)	Biolegend	302028	1:50
anti-CD14 (clone 63D3)	Biolegend	367113	1:50
anti-HLA-DR (clone L243)	Biolegend	307615	1:50
anti-CD11b (clone ICRF44)	Biolegend	301351	1:100
anti-TLR4 (clone HTA125)	Biolegend	312811	1:50
anti-CD206 (clone 15-2)	Biolegend	321140	1:50
anti-CD163 (clone GHI/61)	Biolegend	333630	1:100
anti-TNF (clone MAb11)	Biolegend	502948	1:40
anti-IL-6 (clone MQ2-13A5)	Biolegend	501107	1:40
Antibodies (myeloid cell panel, Syngeneic MB49 urothelial cancer model)			
CD45 (clone 30-F11)	Biolegend	103128	1:100
CD124 (IL-4Ra) (clone I015F8)	Biolegend	144804	1:50
I-a/I-e (clone M5/114.15.2)	Biolegend	107645	1:100
F4/80 (clone BM8)	Biolegend	123147	1:100
CD206 (clone C068C2)	Biolegend	141721	1:200
TNF (clone MP6-XT22)	Biolegend	506345	1:40
IL-10 (clone JES5-16E3)	Thermo Fisher	505022	1:50
Antibodies (lymphoid cell panel, Syngeneic MB49 urothelial cancer model)			
CD45 (clone 30-F11)	Biolegend	103128	1:200
CD25 (clone PC61)	Biolegend	102033	1:100
CD3 (clone 17A2)	Biolegend	100248	1:50
CD4 (clone GK1.5)	Biolegend	100434	1:100
CD8a (clone 53-6.7)	Biolegend	100741	1:100
FOXP3 (clone MF-14)	Biolegend	126406	1:50

Mouse IFN-γ (clone XMG1.2)	Biolegend	505835	1:50
CD69 (clone H1.2F3)	Biolegend	104536	1:100
CD38 (clone 90)	Biolegend	102712	1:100
Reagents/Kits			
Name	**Source**	**#Cat.**	
Protein transport inhibitor cocktail	eBioscience	00-4980-03	
Zombie Aqua™ Fixable Viability Kit	Biolegend	423101	
TruStain FcX™	Biolegend	101320	
Fixation and Permeabilization Buffer Set	Biolegend	421403	
Human TruStain FcX™	Biolegend	422302	
True-Stain Monocyte Blocker™	Biolegend	426102	
2-NBDG Glucose Uptake Assay Kit	Abcam	ab235976	
ELISA			
Mouse ELISA Kits			
TNF- DuoSet	R and D Systems	DY410	
IL-6 DuoSet	R and D Systems	DY406	
IFN- DuoSet	R and D Systems	DY485	
CCL2/JE/MCP-1 DuoSet	R and D Systems	DY479	
LEGEND MAX™ Mouse IFN-β	Biolegend	439407	
Human ELISA Kits			
TNF- DuoSet	R and D Systems	DY210	
IL-6 DuoSet	R and D Systems	DY206	
IFN-β ELISA Kit	PBL Assay Science	41410-2	
Rat ELISA Kits			

IFN- Quantikine	R and D Systems	RIF00
TNF- Quantikine	R and D Systems	RTA00
IL-2 Quantikine	R and D Systems	R2000
Chromatin Immunoprecipitation		
ChIP Antibodies		
Histone H3K9me3 (H3K9 Trimethyl) Polyclonal Antibody	epigentek	A-4036-100
Anti-Histone H3 (tri methyl K4) antibody - ChIP Grade	abcam	ab8580
ChIP Reagents		
BSA	Sigma-Aldrich	A3294
Salmon Sperm DNA	Thermo Fisher Scientific	15632011,
HEPES	Sigma-Aldrich	H3375
Formaldehyde	Sigma-Aldrich	252549
EGTA	Sigma-Aldrich	03777
EDTA	Sigma-Aldrich	E6758
TritonX-100	Sigma-Aldrich)	T8787
SDS	Sigma-Aldrich	71736
NaHCO3	Sigma-Aldrich	5761
Nuclease free water	Thermo Fisher Scientific	AM9930
SYBR green dye	Applied Biosystems	4385614

Supplementary Table. 2: Cloning and PCR primers used in the study

Cloning primers used in the study		
Accession Number	**Gene**	**Sequence (5'-3')**
	pSD5hsp60.MT3692 (F)	GGGCATCATATGCACGCTGTGACTCGTC
	pSD5hsp60.MT3692 (R)	GGGACGCGTTATTGATCGCTGATGGTCGATT
	Kanamycin cassette (F)	GAGAAAACTCACCGAGGCAG
	Kanamycin cassette (R)	GTATTTCGTCTCGCTCAGGC
32287254	*M.tb* sigH (F)	GCGATGGTGGCTTCTCCCTCG
	M.tb sigH (R)	CCATCTTGCACAGCTCGCGTAG
qPCR primers used in the study		
Mouse Primers		
11461	Mouse.β actin (F)	TAAGGCCAACCGTGAAAAGATG
	Mouse.β actin (R)	CTGGATGGCTACGTACATGGCT
21926	Mouse.TNF-α (F)	GACCCTCACACTCAGATCATC
	Mouse.TNF-α (R)	GCTGCTCCTCCACTTGGT
15977	Mouse.IFN-β (F)	CCACAGCCCTCTCCATCAAC
	Mouse.IFN-β (R)	CTCCGTCATCTCCATAGGGA
16193	Mouse.IL6 (F)	CTGCAAGAGACTTCCATCCAG
	Mouse.IL6 (R)	CAGGTCTGTTGGGAGTGG
15978	Mouse.IFN (F)	AGCGGCTGACTGAACTCAGATTGT
	Mouse.IFN (R)	GTCACAGTTTTCAGCTGTATAGGG
16176	Mouse.IL1 (F)	GGAGAGTGTGGATCCCAA
	Mouse.IL1 (R)	GTGGAGTTTGAGTCTGCAG
20296	Mouse.MCP1 (F)	GGCTCAGCCAGATGCAGTTAAC
	Mouse.MCP1 (R)	GATCCTCTTGTAGCTCTCCAGC
16160	Mouse.IL12b (F)	GAAAGACGTTTATGTTGTAGAGG
	Mouse.IL12b (R)	GACTCCATGTCTCTGGTCTG

17329	Mouse.CXCL9 (F)	GGAGTTCGAGGAACCCTAGTG
	Mouse.CXCL9 (R)	GGGATTTGTAGTGGATCGTGC
15945	Mouse.CXCL10 (F)	GTGGGACTCAAGGGATCCCTCTC
	Mouse.CXCL10 (R)	GCTTCCCTATGGCCCTCATTC
18126	Mouse.NOS2 (F)	GTTCTCAGCCCAACAATACAAG
	Mouse.NOS2 (R)	GGAACATTCTGTGCTGTCCC
20299	Mouse.CCL22 (F)	CTCTGATGCAGGTCCCTATGGTG
	Mouse.CCL22 (R)	GGCAGAGGGTGACGGATGTAG
Human Primers		
26827	Human. RNU6A (F)	CTCGCTTCGGCAGCACATATAC
	Human. RNU6A (R)	AATATGGAACGCTTCACGAATTTG
3456	Human.IFNβ (F)	CAACTTGCTTGGATTCCTACAAAG
	Human.IFNβ (R)	TATTCAAGCCTCCCATTCAATTG
3569	Human.IL6 (F)	GGTACATCCTCGACGGCATCT
	Human.IL6 (R)	GTGCCTCTTTGCTGCTTTCAC
Rat Primers		
64367	Rat.PPIB (F)	CAGGATTCATGTGCCAGGGT
	Rat.PPIB (R)	CCAAAGACCACATGCTTGCC
24481	Rat.IFN-β (F)	GAGTCTTCACACTCCTGGC
	Rat.IFN-β (R)	GTCCTTCAGGCATGAGACAG
298210	Rat.IFN–α (F)	GCGTTCCTGCTGTGCTTCTC
	Rat.IFN-α (R)	CCATTCAGCTGCCTCAGGAGC
25712	Rat.IFN–γ (F)	CGTCTTGGTTTTGCAGCTCT
	Rat.IFN-γ (R)	CGTCCTTTTGCCAGTTCCTC
24599	Rat. iNOS (F)	GGTGAGGGGACTGGACTTTTAG
	Rat. iNOS (R)	TTGTTGGGCTGGGAATAGCA
245920	Rat.IP10 (F)	TCCACCTCCCTTTACCCAGT
	Rat.IP10 (R)	AGAGCTAGGAGAGCCGTCAT
24770	Rat.MCP-1 (F)	CAGGTCTCTGTCACGCTTCTG
	Rat.MCP-1 (R)	GCCAGTGAATGAGTAGCAGCAG
25542	Rat.MIP-1α (F)	ACAAGCGCACCCTCTGTTAC
	Rat.MIP-1α (R)	GGTCAGGAAAATGACACCCG

24494	Rat.IL-1β (F)	GACTTCACCATGGAACCCGT
	Rat.IL-1β (R)	GGAGACTGCCCATTCTCGAC
24835	Rat.TNF-α (F)	CGTCCCTCTCATACACTGG
	Rat.TNF-α (R)	CATGCTTTCCGTGCTCATG
59086	Rat.TGF-β (F)	TGACGTCACTGGAGTTGTCC
	Rat.TGF-β (R)	CCTCGACGTTTGGGACTGAT
25325	Rat.IL-10 (F)	CCTCTGGATACAGCTGCGAC
	Rat.IL-10 (R)	TGCCGGGTGGTTCAATTTTTC
ChIP-PCR Primers		
	Human.GAPDH (F)	TACTAGCGGTTTTACGGGCG
	Human.GAPDH (R)	TCGAACAGGAGGAGCAGAGAGCGA
	Human.IL-6 (F)	CGGTGAAGAATGGATGACCT
	Human.IL-6 (R)	AAACGAGACCCTTGCACAAC
	Human.TNF-α (F)	ATCAGTCAGTGGCCCAGAAGACCC
	Human.TNF-α (R)	CCACGTCCCGGATCATGCTTCAG